

HybridFlow: A Two-Step Generative Policy for Robotic Manipulation

Zhenchen Dong², Jinna Fu¹, Jiaming Wu¹, Shengyuan Yu³, Fulin Chen¹, Yide Liu^{1,†}

¹Anker Humanoid Lab ²PolyU ³CUHK

†Corresponding author

Abstract: Limited by inference latency, existing robot manipulation policies lack sufficient real-time interaction capability with the environment. Although faster generation methods such as flow matching are gradually replacing diffusion methods, researchers are pursuing even faster generation suitable for interactive robot control. MeanFlow, as a one-step variant of flow matching, has shown strong potential in image generation, but its precision in action generation does not meet the stringent requirements of robotic manipulation. We therefore propose **HybridFlow**, a **3-stage method** with **2-NFE**: Global Jump in MeanFlow mode, ReNoise for distribution alignment, and Local Refine in ReFlow mode. This method balances inference speed and generation quality by leveraging the rapid advantage of MeanFlow one-step generation while ensuring action precision with minimal generation steps. Through real-world experiments, HybridFlow outperforms the 16-step Diffusion Policy by **15–25%** in success rate while reducing inference time from 152ms to 19ms (**8× speedup, ~52Hz**); it also achieves 70.0% success on unseen-color OOD grasping and 66.3% on deformable object folding. We envision HybridFlow as a practical low-latency method to enhance real-world interaction capabilities of robotic manipulation policies.

Keywords: Imitation Learning, Robotic Manipulation, Few-Step Inference

1 Introduction

Robotic manipulation policies require real-time inference to enable responsive closed-loop control. Recent diffusion-based policies [1, 2] have demonstrated impressive performance, yet their reliance on 8–32 denoising steps results in slow inference. While flow matching methods [3, 4, 5] offer potential speedups by learning continuous transport maps, they typically still require multiple integration steps. This latency bottleneck remains a critical challenge for deploying generative policies in time-sensitive robotic systems.

Under this latency constraint, we naturally focus on methods that require minimal sampling steps. MeanFlow [6, 7] is particularly attractive, as it theoretically supports 1-step inference by learning an average velocity field. Motivated by this efficiency promise, we initially set out to implement MeanFlow for robot manipulation tasks. However, we encountered a critical obstacle: *the validation loss could not reach usable levels during training* (Figure 1). Specifically, while the loss decreased from initialization, it stabilized at $\sim 10^{-3}$ —an order of magnitude higher than multi-step methods achieving $\sim 10^{-4}$. This precision gap translates to unreliable policy behavior in practice. More surprisingly, we discovered that multi-step MeanFlow inference does not improve performance—contradicting the intuition that additional refinement steps should enhance prediction quality. This observation, consistent with findings across multiple domains [8], suggests a fundamental distributional mismatch rather than a simple precision limitation.

Work done during an internship at Anker.

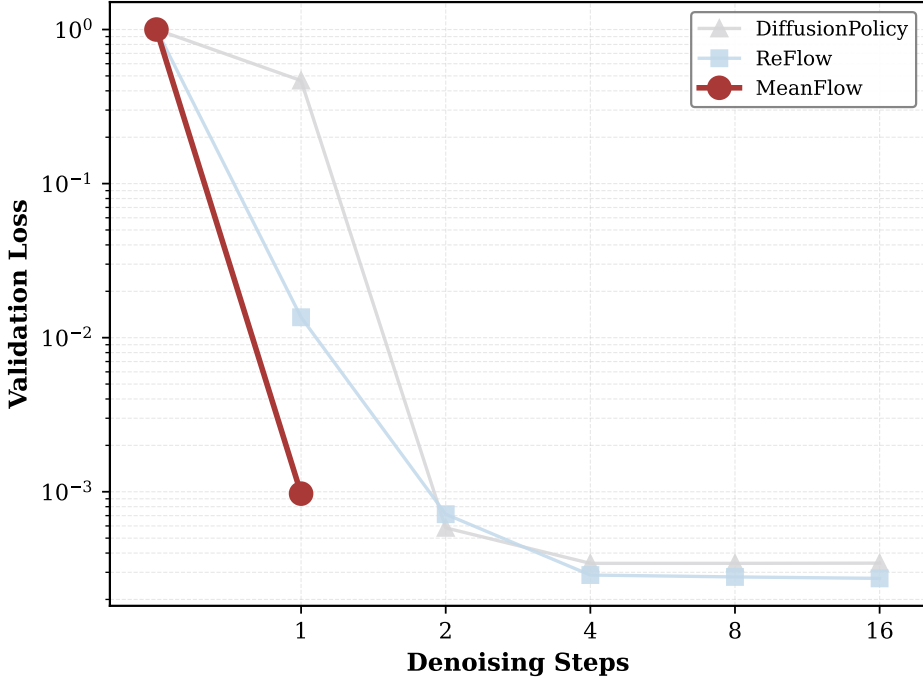


Figure 1: **Validation Loss of MeanFlow Cannot Reach Usable Levels.** Comparison of validation loss across different methods on robot manipulation tasks. While MeanFlow (gray) shows loss reduction from 0-step to 1-step, the achieved loss magnitude ($\sim 10^{-3}$) remains significantly higher than multi-step methods (Diffusion Policy, ReFlow), which converge to $\sim 10^{-4}$ levels. This gap indicates that MeanFlow cannot achieve the precision required for reliable policy performance.

To isolate the source of this failure, we conducted controlled experiments comparing multi-step Diffusion Policy [1] and ReFlow [9] under identical task configurations and training procedures. Remarkably, both methods achieved normal validation loss convergence on the same tasks, indicating that the problem lies not in task difficulty but in the formulation of MeanFlow. These controls rule out task complexity and training setup as primary causes, and support the diagnosis of a formulation-level issue.

These controlled results indicate that what we need is not “more steps” but rather a new inference paradigm that retains the speed advantage of MeanFlow while addressing its precision and distribution consistency issues. While MeanFlow struggles to achieve high accuracy in a single step, its capacity for rapid coarse localization remains intact. This motivates a natural question: *can we leverage MeanFlow for fast global positioning, then refine with a more stable method?* Crucially, we observe that ReFlow and MeanFlow are mathematically related through the MeanFlow identity [6]—when the time interval approaches zero ($r \rightarrow t$), the average velocity $u(z_t, r, t)$ converges to the instantaneous velocity $v(z_t, t)$. This suggests that a single network can serve both purposes by varying its input parameters.

A straightforward idea is to use the coarse prediction of MeanFlow as the starting point for a refinement step. However, the coarse output x_{coarse} exhibits distributional mismatch with the training marginals, causing the refinement to operate in an out-of-distribution (OOD) regime where predictions become unreliable. To address this, we introduce **ReNoise** as a distribution bridge between the two stages. We propose **HybridFlow**, a 3-stage method that trains a single unified model but deploys it in complementary ways: (1) **Global Jump**—use the model in MeanFlow mode for rapid coarse prediction; (2) **ReNoise**—pull the coarse prediction back toward the training distribution via linear interpolation $z_{\text{refine}} = \alpha z_1 + (1 - \alpha)x_{\text{coarse}}$, ensuring the refinement operates in-distribution; (3) **Local Refine**—use the model in ReFlow mode for precise correction from the better-conditioned

state. In plain terms, there are three stages but only two network forward passes: ReNoise is a parameter-free interpolation, not an extra model call. This design achieves 2-NFE (two network evaluations) inference—substantially fewer evaluations than 16-step baselines—while maintaining or exceeding their success rates. Critically, it requires neither separate models nor distillation from a pretrained teacher.

Our contributions are threefold: **(1)** We analyze a key failure mode of MeanFlow in robot manipulation and introduce a HybridFlow strategy to address it. **(2)** Compared to distillation-based approaches, our method achieves faster training by avoiding teacher-student training setups. **(3)** We validate HybridFlow in both simulated and real environments.

2 Related Work

Diffusion-based Manipulation Policies. Diffusion Policy [1] pioneered the application of denoising diffusion probabilistic models (DDPMs) to visuomotor control, framing action generation as a conditional denoising process. By iteratively refining noisy action sequences over 8–16 steps, it achieves strong performance on complex manipulation tasks. Subsequent work extended this to 3D representations [10], enabling better spatial generalization and safety properties. However, these methods inherently require multiple denoising steps, resulting in inference latencies of 50–200ms per action, which limits real-time deployment. Our work addresses this bottleneck through a fundamentally different approach that achieves comparable performance in 2 steps.

Flow Matching for Generative Modeling. Flow matching methods [11] learn continuous transport maps via ordinary differential equations (ODEs), offering a deterministic alternative to stochastic diffusion. Rectified Flow [9] simplifies this by using straight-line paths between noise and data, enabling efficient ODE integration. Recent work has applied flow matching to image generation [12], demonstrating its versatility across domains. MeanFlow [6] introduced average velocity fields to enable one-step generation, achieving state-of-the-art results on ImageNet (FID 3.43 at 1-NFE). Follow-up work extended MeanFlow to latent-free pixel-space generation [13], achieving FID 2.22 at 256×256 resolution by decoupling network output and loss spaces. Beyond images, MeanFlow-style regressors have been applied as first-stage initializers for 3D PDE solvers [14] and target speaker extraction [15], demonstrating cross-domain effectiveness. Concurrent to our work, RMFlow [16] improves 1-NFE MeanFlow for image and molecule generation through noise-injection refinement with likelihood maximization objectives. While both approaches address the distribution mismatch issue of MeanFlow, our work focuses on robot manipulation policies and differs in combining ReNoise with ReFlow’s local refinement mechanism (via the MeanFlow identity $r \rightarrow t$) and analyzing error propagation through Lipschitz constants, whereas RMFlow employs pure noise injection with ELBO-based training. Concretely, our novelty is a single-model method that uses MeanFlow for global jump, uses the $r = t$ ReFlow mode for local refine, and uses ReNoise to keep refinement in-distribution—without distillation. As we show in Section 3, the one-step formulation of MeanFlow struggles in robot manipulation settings, and multi-step refinement fails to recover performance—motivating our hybrid approach.

Few-step Generation via Distillation and Consistency. A parallel line of work accelerates diffusion models through distillation [17, 18] or consistency training [19]. Consistency Policy [20] distills pre-trained Diffusion Policies into single-step generators, achieving $40 \times$ speedup (1.5Hz \rightarrow 62Hz). Similarly, ManiCM [21] and OneDP [22] apply consistency models to 3D manipulation, reducing inference to one forward pass. Shortcut Models [23] condition on desired step counts during training to enable variable-step inference without distillation. An alternative approach combines MeanFlow with reinforcement learning: DMPO [24] achieves 120Hz real-time control on manipulation benchmarks through dispersive regularization and policy fine-tuning. While these methods achieve impressive speedups, distillation-based approaches require expensive teacher-student training setups. In contrast, HybridFlow achieves few-step inference through inference-time orchestration of a single end-to-end trained model, without distillation or auxiliary sampling procedures.

Coarse-to-Fine and Hierarchical Control. Our two-stage design relates to coarse-to-fine strategies in motion planning [25] and hierarchical reinforcement learning [26], where high-level policies propose waypoints refined by low-level controllers. Hierarchical Diffusion Policy [27] decomposes manipulation into high-level pose prediction and low-level trajectory generation. However, these methods typically involve separate models or training stages. HybridFlow differs fundamentally: rather than learning a hierarchical decomposition, we exploit the mathematical connection between average and instantaneous velocities (via the MeanFlow identity) to use a *single* model in two inference modes, connected by a distribution-aware re-noise bridge. This design is conceptually simpler and requires no architectural or training modifications beyond standard MeanFlow.

3 Hybrid Flow

Problem Setup and Notation. We learn a visuomotor policy mapping observations $o \in \mathcal{O}$ to action trajectories $x \in \mathbb{R}^d$. Following flow-based approaches [9, 6], we formulate this as learning $p(x|c)$, where $c = f_\phi(o)$ is the observation encoding (subscript ϕ denotes encoder parameters). Throughout, we use: (1) subscript t for continuous time $t \in [0, 1]$ (e.g., Z_t, q_t), (2) superscript (k) for discrete iteration steps (e.g., $z^{(k)}$), (3) subscript θ for model parameters, and (4) $*$ for oracle/true quantities (e.g., $u^*, z_*^{(k)}$).

Flow Matching Background. Flow-based generative models learn a transport map connecting a simple noise distribution $\pi_1 = \mathcal{N}(0, I)$ to the data distribution $\pi_0 = p_{\text{data}}(x|c)$ via a continuous-time ordinary differential equation (ODE):

$$\frac{dZ_t}{dt} = v(Z_t, t, c), \quad t \in [0, 1], \quad Z_1 \sim \pi_1, \quad Z_0 \sim \pi_0 \quad (1)$$

where $v(\cdot, t, c)$ is the velocity field at time t conditioned on c . Rectified Flow [9] simplifies this by using straight-line interpolation $Z_t = (1-t)X_0 + tX_1$, leading to a constant velocity $v^* = X_1 - X_0$.

MeanFlow Formulation. MeanFlow [6] introduces the concept of *average velocity* over an interval $[r, t]$:

$$u(z_t, r, t, c) \triangleq \frac{1}{t-r} \int_r^t v(z_\tau, \tau, c) d\tau \quad (\text{for } r \neq t) \quad (2)$$

Through the MeanFlow identity (differentiating the integral), this relates to the instantaneous velocity:

$$u(z_t, r, t, c) = v(z_t, t, c) - (t-r) \frac{d}{dt} u(z_t, r, t, c) \quad (3)$$

Critically, taking the limit $r \rightarrow t$ in the definition yields:

$$u(z_t, t, t, c) \triangleq \lim_{r \rightarrow t} u(z_t, r, t, c) = v(z_t, t, c) \quad (4)$$

This identity establishes that when $r = t$, the average velocity coincides with the instantaneous velocity, enabling a single network u_θ to serve both purposes. For one-step generation, MeanFlow uses:

$$\hat{x}(z_1, c) = z_1 - u_\theta(z_1, 0, 1, c) \quad (5)$$

Why Multi-step MeanFlow Does Not Improve Performance. Intuitively, multi-step refinement should improve precision:

$$z^{(k+1)} = z^{(k)} - u_\theta(z^{(k)}, t_k, t_{k+1}, c), \quad k = 0, \dots, K-1 \quad (6)$$

However, as shown in Figure 1, this does not occur in practice—additional steps provide no significant improvement. This phenomenon has been empirically observed across multiple domains [8]: Ai et al. report that on CIFAR-10, MeanFlow achieves FID 2.80 at 1-step but degrades to FID 5.14 at 4-steps and FID 4.34 at 8-steps, with negative log-likelihood deteriorating from -9.00 (8-step) to -97.59 (1-step), demonstrating that multi-step MeanFlow inference does not improve performance. We explain this via error propagation analysis. Let $e_k = u_\theta(z^{(k)}, t_k, t_{k+1}, c) - u^*(z^{(k)}, t_k, t_{k+1}, c)$ denote the one-step approximation error at the current (possibly off-track) state. Following standard

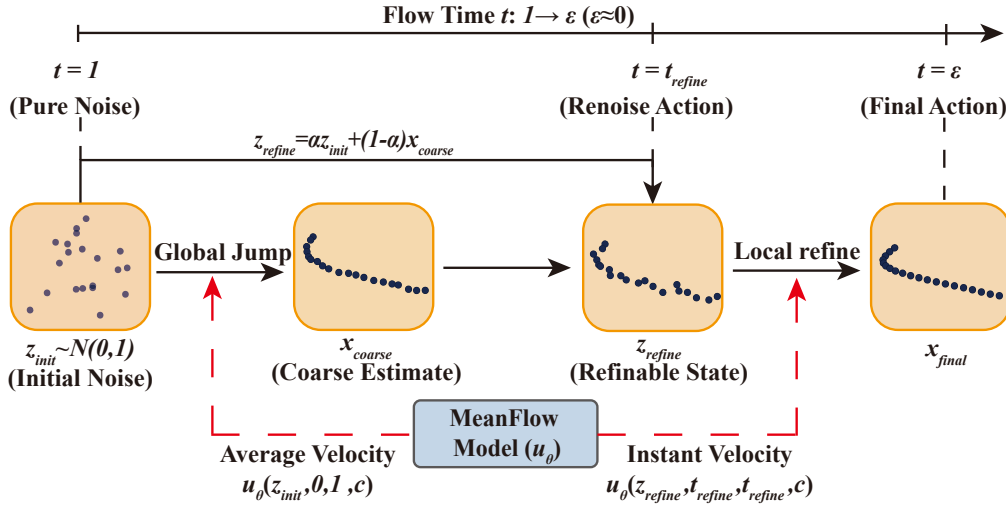


Figure 2: **HybridFlow Inference Mechanism.** Illustration of our 3-stage method with 2-NFE: (1) Global Jump uses MeanFlow mode ($r = 0, t = 1$) for fast coarse prediction, (2) ReNoise pulls the prediction back into training distribution via controlled noise injection, (3) Local Refine uses ReFlow mode ($r = t$) for precise correction. The method requires only two network forward passes (NFE=2), with ReNoise being a parameter-free interpolation stage.

ODE analysis [28], we assume both the learned velocity field u_θ and the true velocity field u^* are locally L -Lipschitz continuous in their first arguments (sufficient conditions for well-posedness and error propagation). Under these assumptions:

$$\begin{aligned}
\|z^{(k+1)} - z_*^{(k+1)}\| &= \|(z^{(k)} - u_\theta(z^{(k)}, \dots)) - (z_*^{(k)} - u^*(z_*^{(k)}, \dots))\| \\
&\leq \|z^{(k)} - z_*^{(k)}\| + \|u_\theta(z^{(k)}, \dots) - u^*(z_*^{(k)}, \dots)\| \\
&\leq \|z^{(k)} - z_*^{(k)}\| + \|u_\theta(z^{(k)}, \dots) - u^*(z^{(k)}, \dots)\| \\
&\quad + \|u^*(z^{(k)}, \dots) - u^*(z_*^{(k)}, \dots)\| \\
&\leq \|z^{(k)} - z_*^{(k)}\| + \|e_k\| + L\|z^{(k)} - z_*^{(k)}\| \\
&= (1 + L)\|z^{(k)} - z_*^{(k)}\| + \|e_k\|
\end{aligned} \tag{7}$$

Unrolling this recursion yields:

$$\|z^{(K)} - z_*^{(K)}\| \lesssim \sum_{k=0}^{K-1} (1 + L)^{K-1-k} \|e_k\| \tag{8}$$

This shows early errors are amplified exponentially by $(1 + L)^{K-1-k}$. Crucially, the Lipschitz constant L itself grows significantly as sampling progresses toward the data distribution [29]—when noise diminishes and the distribution becomes sharper, the velocity field exhibits heightened sensitivity to perturbations. Simultaneously, as $z^{(k)}$ deviates from the training distribution due to accumulated errors, the model operates in an OOD regime where $\|e_k\|$ increases [30]. This distribution shift can be quantified as:

$$\text{Shift}(k) \triangleq D_{\text{KL}}(\mathcal{L}(z^{(k)}) \| q_{t_k}) \tag{9}$$

where q_t is the training-time marginal at time t . The combination of (1) growing L , (2) exponential error amplification, and (3) increasing per-step error $\|e_k\|$ due to distribution drift explains why multi-step refinement fails to improve—and sometimes degrades—performance.

HybridFlow: Two-Stage Inference. Our key insight is to avoid sequential error accumulation by separating global and local transport, connected via a distribution-aware bridge. As illustrated in Figure 2, HybridFlow uses a 3-stage method with 2-NFE:

Step 1: Global Jump. Use the model in MeanFlow mode to perform a single large jump from noise to the vicinity of the target:

$$x_{\text{coarse}} = z_1 - u_\theta(z_1, 0, 1, c) \quad (10)$$

This leverages the ability of MeanFlow to predict the average displacement over the entire path $[0, 1]$. While computationally efficient, x_{coarse} exhibits reduced precision and may fall outside the support of the training distribution q_0 , as empirically observed in prior work [8].

Step 2: ReNoise. To enable effective refinement, we pull x_{coarse} back toward the training distribution via linear interpolation:

$$z_{\text{refine}} = \alpha z_1 + (1 - \alpha)x_{\text{coarse}} \quad (11)$$

This can equivalently be written as $z_{\text{refine}} = x_{\text{coarse}} + \alpha(z_1 - x_{\text{coarse}})$, explicitly showing that ReNoise adds noise linearly. Here, $\alpha \in (0, 1)$ controls the re-noising strength. In our setting, denoising from noise to action is computed from MeanFlow average velocity, under which time and noise level are linearly coupled along the Rectified Flow interpolation path. Since both time and noise strength are normalized to $(0, 1)$, we set $\alpha = t_{\text{refine}}$, so the injected noise strength is matched to the corresponding refinement time and to the training marginal $q_{t_{\text{refine}}}$. This design balances two objectives: (1) retaining semantic information from x_{coarse} , and (2) ensuring the refinement step operates within the model’s training distribution.

Step 3: Local Refine. From the better-conditioned state z_{refine} , we apply a local refinement using the model with $r = t$:

$$x_{\text{final}} = z_{\text{refine}} - u_\theta(z_{\text{refine}}, t_{\text{refine}}, t_{\text{refine}}, c) \quad (12)$$

By Eq. 4, $u_\theta(z_{\text{refine}}, t_{\text{refine}}, t_{\text{refine}}, c)$ equals the instantaneous velocity $v_\theta(z_{\text{refine}}, t_{\text{refine}}, c)$. This enables precise local corrections within the training distribution without accumulating multi-step errors. Note that during training, the network u_θ is trained with the MeanFlow objective using Jacobian-Vector Product (JVP) to compute the derivative term in Eq. 3, ensuring well-defined gradients even when $r = t$.

Why ReNoise Works: Distribution Alignment Intuition. ReNoise aims to mitigate the distribution shift that plagues multi-step inference. The key intuition is as follows: if x_{coarse} exhibits systematic bias or falls in a low-density region of q_0 , directly refining it causes u_θ to operate out-of-distribution. By interpolating with noise $z_1 \sim \mathcal{N}(0, I)$, we construct z_{refine} whose marginal distribution is expected to better align with the training marginal $q_{t_{\text{refine}}}$, thereby improving the reliability of the subsequent refinement step.

To understand the choice of α , we provide a variance-matching intuition, though we emphasize this is a heuristic rather than a rigorous derivation. The general variance formula for the linear combination $z_{\text{refine}} = \alpha z_1 + (1 - \alpha)x_{\text{coarse}}$ is:

$$\text{Var}(z_{\text{refine}}) = \alpha^2 \text{Var}(z_1) + (1 - \alpha)^2 \text{Var}(x_{\text{coarse}}) + 2\alpha(1 - \alpha)\text{Cov}(z_1, x_{\text{coarse}}) \quad (13)$$

In our implementation, we *reuse* the same noise sample z_1 from the Global Jump step (Eq. 10), meaning $x_{\text{coarse}} = z_1 - u_\theta(z_1, 0, 1, c)$ is deterministically derived from z_1 . Consequently, $\text{Cov}(z_1, x_{\text{coarse}}) \neq 0$ in general, and the covariance term cannot be ignored rigorously [31]. However, if we hypothetically considered a scenario where z_1 were freshly sampled (independent of the z_1 used to generate x_{coarse}), the covariance would vanish, yielding:

$$\text{Var}(z_{\text{refine}}) \approx \alpha^2 \text{Var}(z_1) + (1 - \alpha)^2 \text{Var}(x_{\text{coarse}}) \quad (14)$$

Under this idealized independence approximation, and noting that $\text{Var}(z_1) \approx 1$ while $\text{Var}(x_{\text{coarse}})$ is typically small (actions lie in a compact normalized space), the dominant contribution comes from the α^2 term. This motivates the heuristic $\alpha = t_{\text{refine}}$: by setting the mixing coefficient equal to the refinement time, we aim to match the marginal variance $\text{Var}(z_{\text{refine}})$ to the expected variance $\text{Var}(q_{t_{\text{refine}}})$ in the training distribution [32]. While this reasoning involves simplifying assumptions (ignoring the covariance term and assuming approximate variance scales), it provides an intuitive connection between the re-noising strength and the ODE time parameter. In practice, the optimal value of α (and thus t_{refine}) depends on noise schedule parameterization, action space normalization, and the learned velocity field geometry, and is therefore determined empirically through ablation studies (Section 4).

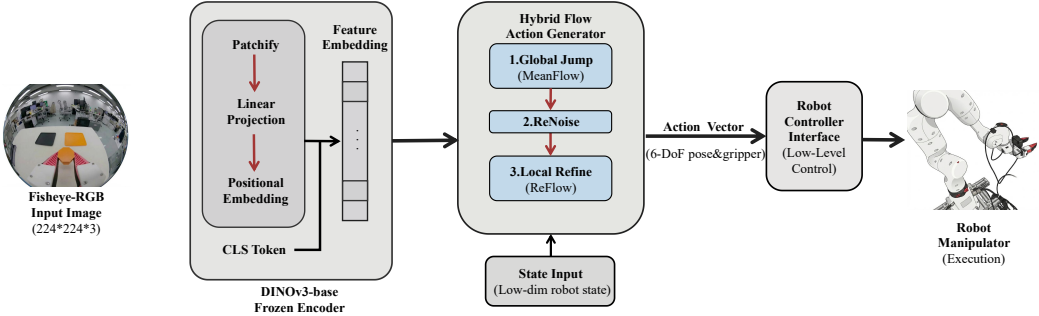


Figure 3: **HybridFlow System Architecture.** The system processes fisheye RGB observations through a DINOv3 encoder to generate condition embeddings, which guide the HybridFlow action generator through a 3-stage method with 2-NFE: (1) Global Jump using MeanFlow mode for coarse prediction, (2) ReNoise to pull the prediction back into training distribution, and (3) Local Refine using ReFlow mode for precise correction. The final action trajectory is executed by the robot controller.

4 Experiments

Task Definitions. We evaluate HybridFlow on 4 simulation tasks and 2 categories of real-robot manipulation tasks. *Simulation tasks* are drawn from RoboMimic [33] benchmark: (1) *Can* (pick-and-place with alignment), (2) *Lift* (vertical grasping), (3) *Square* (precise peg-in-hole insertion), and (4) *Transport* (dual-arm coordination). *Real-robot tasks* comprise two categories: (a) *Colored object grasping*, where the policy must grasp and place rigid objects across three color variations (Black and Orange for training, Pink for out-of-distribution generalization testing), probing visual robustness under appearance shifts; (b) *Eyepatch folding*, a deformable object manipulation task requiring sequential dual-point grasping and coordinated folding motions, testing the policy’s ability to handle non-rigid dynamics and multi-stage contact-rich operations beyond standard pick-and-place scenarios.

Simulation Setup. All simulation experiments are conducted in MuJoCo with a Vision Transformer (ViT) encoder. Observations consist of multi-view RGB images ($84 \times 84 \times 3$ per camera, 3 cameras). Actions are 6-DoF end-effector poses plus gripper commands. Training and inference are performed on NVIDIA RTX 5090 GPU. Each method is evaluated over 100 episodes per task. Baselines (all run for 1–32 steps): Diffusion Policy [1] (DDIM), ReFlow [9], and ShortCut Flow [23].

Real Robot Setup. Physical experiments use a 7-DoF robotic arm with parallel gripper, deployed on the NVIDIA Jetson AGX Thor platform for on-device inference. The setup follows Universal Manipulation Interface (UMI)[34] protocol with fisheye RGB camera ($224 \times 224 \times 3$). Tasks involve grasping colored objects with systematic appearance variation to probe out-of-distribution generalization, and eyepatch folding to test deformable object manipulation capabilities. Baseline: Diffusion Policy (16-step DDIM), as it represents the established standard for real-robot manipulation policies.

ReNoise Ratio Selection. The ReNoise ratio α (equivalently, t_{refine}) controls the balance between preserving the coarse prediction’s semantic information and pulling it back toward the training distribution (Section 3). Figure 4 shows validation loss across different α values. We observe that α values that are too small ($\alpha < 0.10$) fail to adequately correct the distribution mismatch, resulting in high validation loss (0.013 at $\alpha = 0.05$). Conversely, values that are too large ($\alpha > 0.25$) introduce excessive noise, degrading the coarse prediction’s quality and increasing loss. The optimal range is $\alpha \in [0.15, 0.20]$, achieving validation loss of 4×10^{-4} . We use $\alpha = 0.15$ throughout our experiments as it provides robust performance across tasks while maintaining a small noise injection level.

Simulation Results. Figure 5 presents success rates across four RoboMimic benchmark tasks as a function of inference steps. HybridFlow achieves competitive performance with only 2 steps,

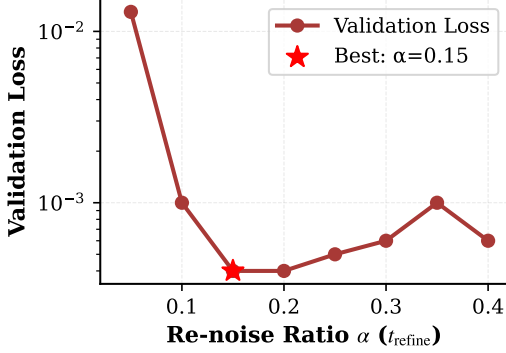


Figure 4: **ReNoise Ratio Ablation.** Validation loss vs ReNoise ratio $\alpha (t_{\text{refine}})$. The optimal range is $\alpha \in [0.15, 0.20]$, balancing distribution alignment and semantic preservation. Too small (< 0.10) fails to correct distribution mismatch; too large (> 0.25) introduces excessive noise.

Table 1: **Real Robot Experimental Results.** Success rates and inference timing comparison between HybridFlow and Diffusion Policy baseline. All models trained on approximately 300 demonstrations.

Task	Condition	HybridFlow	Diffusion Policy	Improvement
Pick-and-Place	In-Distribution	69/80 (86.3%)	51/80 (63.8%)	+22.5%
	OOD (Pink)	14/20 (70.0%)	9/20 (45.0%)	+25.0%
	Inference Time	19ms (~52Hz)	152ms (~6.6Hz)	8× faster
Fabric Folding	Success Rate	53/80 (66.3%)	41/80 (51.3%)	+15.0%
	Inference Time	19ms (~52Hz)	~152ms (~6.6Hz)	8× faster

matching or exceeding multi-step baselines on most tasks. Detailed quantitative analysis is provided in the supplementary material. These controlled simulation experiments validate our method’s effectiveness before real-world deployment.

Real Robot Results: Pick-and-Place. Figure 6 and Table 1 present results on colored object grasping. HybridFlow achieves 86.3% success rate on in-distribution tasks (69/80 trials) and maintains 70.0% on OOD generalization to unseen Pink objects (14/20 trials), significantly outperforming Diffusion Policy’s 63.8% and 45.0% respectively. The OOD performance demonstrates robust visual feature learning through the DINOv3 encoder, with HybridFlow showing **25% absolute improvement** in generalization over the baseline. Critically, HybridFlow achieves these results with **8× faster inference** (19ms vs 152ms), enabling real-time control at $\sim 52\text{Hz}$ on edge hardware. Analysis of failure modes reveals that errors primarily occur when the gripper contacts object edges, causing the object to slip or tumble—a challenge common to both methods but less frequent in HybridFlow due to more precise action predictions.

Real Robot Results: Fabric Manipulation. Figure 7 and Table 1 present results on eyepatch folding, a challenging deformable object manipulation task. HybridFlow achieves 66.3% success rate (53/80 trials), outperforming Diffusion Policy’s 51.3% (41/80 trials) by 15% absolute improvement. This task is particularly demanding as it involves non-rigid dynamics, self-occlusion during folding, continuous shape deformation, and precise dual-point grasping coordination. Analysis of failure modes reveals that errors primarily occur during the second grasp (right edge): imprecise localization while holding the left edge leads to failed grasp attempts, causing the entire subsequent folding sequence to fail. This highlights a key challenge in fabric manipulation where errors cascade through multi-stage contact-rich operations. Despite this difficulty, HybridFlow’s higher success rate demonstrates more robust action prediction under partial observability. Notably, HybridFlow maintains the same 19ms inference time on this complex task, showing that our method’s efficiency is task-agnostic. Both methods were trained on approximately 300 demonstrations, confirming that the performance gap stems from the inference mechanism rather than data scale.

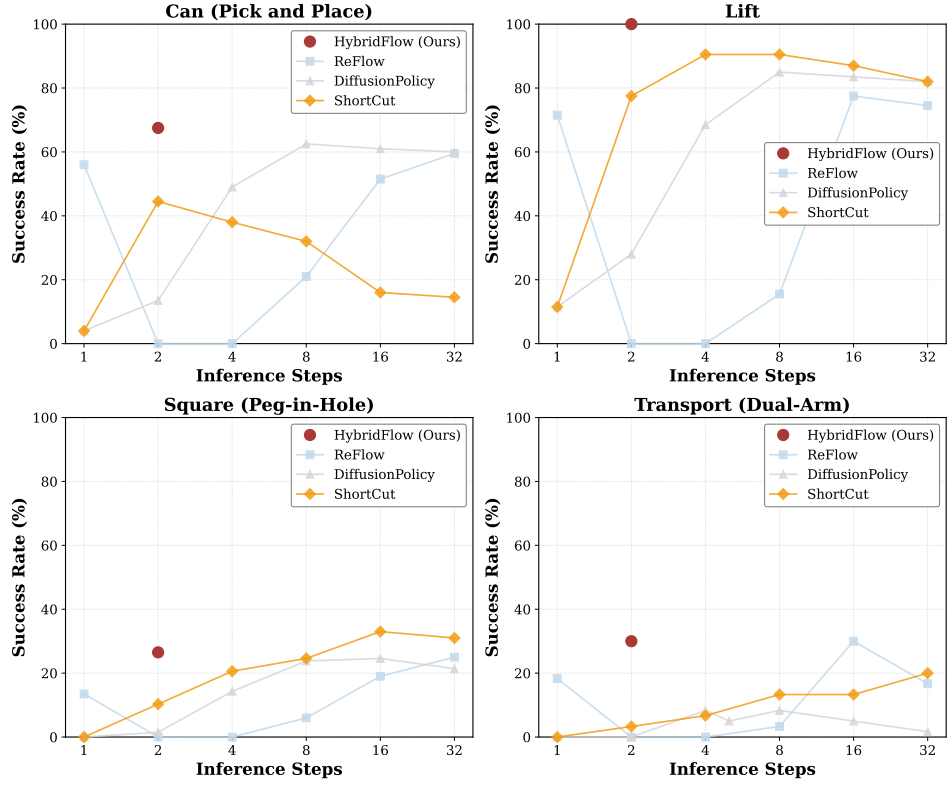


Figure 5: **Simulation Results.** Success rate vs inference steps on four RoboMimic benchmark tasks (Lift, Can, Square, Transport). HybridFlow (red points, 2-NFE) achieves competitive performance compared to multi-step baselines: Diffusion Policy (gray, 16+ steps), ReFlow (blue), and ShortCut (orange). Our method demonstrates that a 3-stage method with 2-NFE can match or exceed the accuracy of methods requiring 8–16 steps, validating our distribution alignment approach in controlled simulation environments.

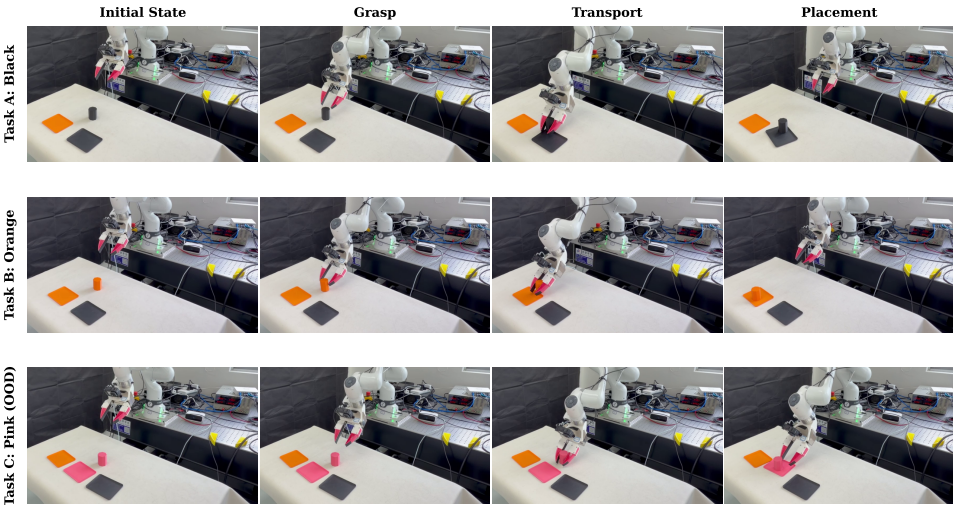


Figure 6: **Real Robot Results: Pick-and-Place.** Execution snapshots for three colored object grasping tasks. Each row shows Initial State → Grasp → Transport → Placement. Training on Black and Orange, testing on Pink (OOD).

Efficiency Analysis. As shown in Table 1, HybridFlow achieves **8 \times speedup** over Diffusion Policy (19ms vs 152ms per action), enabling real-time control at approximately 52Hz on the NVIDIA

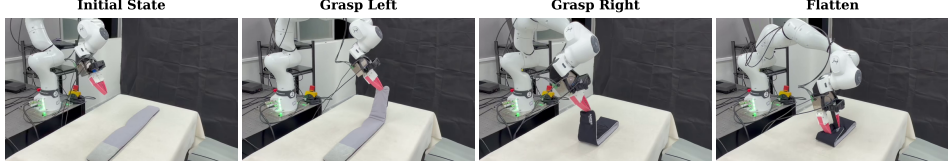


Figure 7: **Real Robot Results: Fabric Manipulation.** Eyepatch folding task demonstrating HybridFlow’s applicability to deformable object manipulation. The policy executes a 4-stage sequence: (1) Initial State with flat eyepatch, (2) Grasp left edge, (3) Grasp right edge while holding left, (4) Fold and flatten. This task involves non-rigid dynamics and dual-arm coordination, showcasing the versatility of our approach beyond rigid object manipulation.

Jetson AGX Thor platform. This dramatic reduction in latency—from 152ms to 19ms—is critical for reactive manipulation tasks where environmental dynamics change rapidly. The efficiency gain comes from reducing inference from 16 DDIM steps to our 3-stage method with 2-NFE, while *improving* task success rates by 15–25%. Importantly, this speedup is achieved without distillation or model compression: both methods use comparable model sizes, demonstrating that our inference-time orchestration is fundamentally more efficient than iterative denoising.

5 Conclusion

This paper studies a practical failure case of MeanFlow in robotic manipulation: higher sampling steps do not reliably recover performance once predictions drift from the training distribution. To address this, we propose HybridFlow, a 3-stage method (Global Jump, ReNoise, and Local Refine) with 2-NFE that combines fast coarse transport with in-distribution local correction using a single model.

Across simulation and real-robot tasks, HybridFlow improves success rates by 15–25% over 16-step Diffusion Policy while reducing inference time from 152ms to 19ms (8× speedup, \sim 52Hz). On real hardware, it achieves 86.3% success on pick-and-place, 70.0% on unseen-color OOD grasping, and 66.3% on deformable-object folding. These results indicate that inference-time orchestration can improve both latency and control quality without distillation or architectural expansion.

Current limitations include task-dependent tuning of the ReNoise ratio α and remaining failures in high-precision contact transitions. Future work will focus on adaptive refinement scheduling, confidence-aware α selection, and integration with online replanning under dynamic disturbances.

References

- [1] C. Chi, S. Feng, Y. Du, Z. Xu, E. Cousineau, B. Burchfiel, and S. Song. Diffusion policy: Visuomotor policy learning via action diffusion. In *Robotics: Science and Systems (RSS)*, 2023.
- [2] Y. Ze, G. Zhang, K. Zhang, C. Hu, M. Wang, and H. Xu. 3d diffusion policy: Generalizable visuomotor policy learning via simple 3d representations. *arXiv preprint arXiv:2403.03954*, 2024. Also known as DP3.
- [3] P. I. Team. π_0 : A vision-language-action flow model for general robot control. *arXiv preprint arXiv:2410.24164*, 2024.
- [4] P. I. Team. $\pi_{0.5}$: a vision-language-action model with open-world generalization. *arXiv preprint arXiv:2504.16054*, 2024.
- [5] R. Team. Rdt2: Enabling zero-shot cross-embodiment generalization by scaling up umi data, September 2025. URL <https://github.com/thu-ml/RDT2>.
- [6] Z. Geng, M. Deng, X. Bai, J. Z. Kolter, and K. He. Mean flows for one-step generative modeling. In *Advances in Neural Information Processing Systems (NeurIPS)*, 2025.
- [7] Z. Geng, Y. Lu, Z. Wu, E. Shechtman, J. Z. Kolter, and K. He. Improved mean flows: On the challenges of fastforward generative models. *arXiv preprint arXiv:2512.02012*, 2025. URL <https://arxiv.org/abs/2512.02012>.
- [8] X. Ai, Y. He, A. Gu, R. Salakhutdinov, J. Z. Kolter, N. M. Boffi, and M. Simchowitz. Joint distillation for fast likelihood evaluation and sampling in flow-based models. *arXiv preprint arXiv:2512.02636*, 2025.
- [9] X. Liu, C. Gong, and Q. Liu. Flow straight and fast: Learning to generate and transfer data with rectified flow. In *International Conference on Learning Representations (ICLR)*, 2023.
- [10] Y. Ze, G. Zhang, K. Zhang, C. Hu, M. Wang, and H. Xu. 3d diffusion policy: Generalizable visuomotor policy learning via simple 3d representations. In *Robotics: Science and Systems (RSS)*, 2024.
- [11] Y. Lipman, R. T. Q. Chen, H. Ben-Hamu, M. Nickel, and M. Le. Flow matching for generative modeling. In *International Conference on Learning Representations (ICLR)*, 2023.
- [12] S. Lee, Z. Lin, and G. Fanti. Improving the training of rectified flows. *arXiv preprint arXiv:2405.20320*, 2024.
- [13] Y. Lu, S. Lu, Q. Sun, H. Zhao, Z. Jiang, X. Wang, T. Li, Z. Geng, and K. He. One-step latent-free image generation with pixel mean flows, 2026.
- [14] Z. Shen, Z. Wang, J. Xin, and Z. Zhang. Two-step diffusion: Fast sampling and reliable prediction for 3d keller-segel and kpp equations in fluid flows. *arXiv preprint arXiv:2601.20024*, 2026.
- [15] R. Shimizu, X. Jiang, and N. Mesgarani. Meanflow-tse: One-step generative target speaker extraction with mean flow. *arXiv preprint arXiv:2512.18572*, 2025.
- [16] Y. Huang, S.-H. Wang, A. L. Bertozzi, and B. Wang. Rmflow: Refined mean flow by a noise-injection step for multimodal generation. 2026. *arXiv:2602.00849*.
- [17] Y. Song, P. Dhariwal, M. Chen, and I. Sutskever. Consistency models. *arXiv preprint arXiv:2303.01469*, 2023.
- [18] T. Salimans and J. Ho. Progressive distillation for fast sampling of diffusion models. *arXiv preprint arXiv:2202.00512*, 2022.

- [19] Y. Song and P. Dhariwal. Improved techniques for training consistency models. *arXiv preprint arXiv:2310.14189*, 2023.
- [20] A. Prasad, K. Lin, J. Wu, L. Zhou, and J. Bohg. Consistency policy: Accelerated visuomotor policies via consistency distillation. *arXiv preprint arXiv:2405.07503*, 2024.
- [21] G. Chen, K. Wang, J. Liu, Z. Che, Y. Cui, S. Zhang, Y. Chang, and J. Tang. Manicm: Real-time 3d diffusion policy via consistency model for robotic manipulation. *arXiv preprint arXiv:2406.01586*, 2024.
- [22] Z. Wang, Z. Li, A. Mandlekar, Z. Xu, J. Tremblay, Y.-W. Chao, S. Birchfield, B. Wen, M. Zhou, M.-Y. Liu, and D. Fox. One-step diffusion policy: Fast visuomotor policies via diffusion distillation. *arXiv preprint arXiv:2410.21257*, 2024.
- [23] K. Frans, D. Hafner, S. Levine, and P. Abbeel. Shortcut models for inexpensive diffusion. *arXiv preprint arXiv:2410.00339*, 2024.
- [24] G. Zou, H. Wang, H. Wu, Y. Qian, Y. Wang, and W. Li. One step is enough: Dispersive meanflow policy optimization. *arXiv preprint arXiv:2601.20701*, 2026.
- [25] R. Tedrake, I. R. Manchester, M. Tobenkin, and J. W. Roberts. Lqr-trees: Feedback motion planning via sums-of-squares verification. *The International Journal of Robotics Research*, 29(8):1038–1052, 2010.
- [26] O. Nachum, S. Gu, H. Lee, and S. Levine. Data-efficient hierarchical reinforcement learning. In *Advances in Neural Information Processing Systems (NeurIPS)*, 2018.
- [27] X. Ma, S. Patidar, I. Haughton, and S. James. Hierarchical diffusion policy for kinematics-aware multi-task robotic manipulation. In *Conference on Computer Vision and Pattern Recognition (CVPR)*, 2024.
- [28] R. T. Q. Chen, R. Gao, I. Kemelmacher-Shlizerman, B. Karrer, and A. G. Dimakis. The probability flow ode is provably fast. In *Advances in Neural Information Processing Systems (NeurIPS)*, 2023.
- [29] T. Mooney and S. H. Kang. Global well-posedness and convergence analysis of score-based generative models via sharp lipschitz estimates. *arXiv preprint arXiv:2405.16104*, 2024.
- [30] T. Zhou, Y. Luo, A. Yu, and W. Chen. An error analysis of flow matching for deep generative models. *OpenReview preprint*, 2025.
- [31] The Book of Statistical Proofs. Variance of the linear combination of random variables. <https://statproofbook.github.io/P/var-lincomb.html>. Accessed: 2026-01-29.
- [32] J. Ho, A. Jain, and P. Abbeel. Denoising diffusion probabilistic models. In *Advances in Neural Information Processing Systems (NeurIPS)*, 2020.
- [33] A. Mandlekar, D. Xu, J. Wong, S. Nasiriany, C. Wang, R. Kulkarni, L. Fei-Fei, S. Savarese, Y. Zhu, and R. Martín-Martín. What matters in learning from offline human demonstrations for robot manipulation. In *Conference on Robot Learning (CoRL)*, 2021.
- [34] C. Chi, Z. Xu, C. Pan, E. Cousineau, B. Burchfiel, S. Feng, R. Tedrake, and S. Song. Universal manipulation interface: In-the-wild robot teaching without in-the-wild robots. In *Proceedings of Robotics: Science and Systems (RSS)*, 2024.